Shahrood University of Technology

Journal of Mining and Environment (JME)

Journal homepage: www.jme.shahroodut.ac.ir

Iranian Society of Mining Engineering (IRSME)

Parametric Optimization of Methane Drainage via Cross-measure Boreholes in Floor Strata of a Coal Mine: A Multiphysics Simulation Study

Tingze Li[1], Yu Wang[2], and Genyuan Tan[3*]

1. Faculty of Geosciences and Engineering, Southwest Jiaotong University, Chengdu, Sichuan, China
2. School of Resources and Geosciences, China University of Mining and Technology, Xuzhou, Jiangsu, China
3. College of Safety Engineering, China University of Mining and Technology, Xuzhou, Jiangsu, China

Article Info

Received 19 August 2025
Received in Revised form 10 October 2025
Accepted 4 January 2025
Published online 4 January 2025

DOI: 10.22044/jme.2026.16664.3273

Keywords

Coal mine gas control
Floor strata
Cross-measure boreholes
Borehole parameter optimization
Stress-permeability coupling

Abstract

Effective gas drainage in coal mines necessitates the precise optimization of borehole parameters to reduce gas pressure and prevent gas outbursts. However, current drilling designs predominantly rely on field experience rather than site-specific quantitative analysis of geological conditions, leading to limitations in adaptability. This study establishes a COMSOL-based multiphysics coupling model that integrates stress-permeability interactions, gas adsorption-desorption kinetics, and fracture-induced permeability evolution to evaluate the gas drainage performance of cross-measure boreholes in floor strata. Simulation results indicate that directional borehole spacing is the most influential factor: reducing the spacing from 25 m to 20 m significantly increases gas drainage efficiency by 31.4%, while extending the drainage duration from 90 days to 270 days expands the influence radius by more than 35%. In contrast, variations in borehole diameter (75-115 mm) and negative pressure (10-90 kPa) exert a negligible impact on gas pressure (with a variation of less than 5%), reflecting limited sensitivity. The optimal borehole location is determined to be at the lower boundary of the mining-induced fracture zone. A gradient layer analysis further confirms that the perforation depth should match the range of the plastic deformation zone (15-25 m). The proposed parametric optimization strategy provides a quantitative framework for directional drilling design, enabling the matching of borehole layout with the scale of fracture development. These findings contribute to enhancing the accuracy of gas control and the engineering adaptability of gas drainage systems under complex geological conditions.

1. Introduction

Gas control is a critical challenge for coal mine safety and green mining. According to the International Labour Organization (ILO), gas explosions account for more than 40% of major coal mine accidents worldwide. Additionally, methane emissions from underground coal mines significantly contribute to global greenhouse gas emissions, reaching over 40 million tons of CO_2-equivalent annually [1,2,3]. In China, floor strata with low permeability and high gas content frequently pose challenges to gas drainage in longwall mining faces. To address this issue, cross-measure boreholes have been widely adopted in practice. However, most borehole layout designs still rely heavily on field experience and lack systematic optimization that considers geological conditions and stress-seepage coupling effects. Field data from Qidong Mine indicate that inappropriate borehole placement can result in a gas pressure reduction rate of less than 25% after 180 days, which falls well below the safe threshold requirement. Nevertheless, methane emissions associated with coal mining remain a primary source of mine disasters-they not only pose severe

Corresponding author: 18955462692@163.com (Genyuan Tan)

threats to the safety of highgas mines and outburst-prone coal seams but also act as a critical barrier to the efficient production of mining faces [4,5,6]. To effectively mitigate methane-related hazards, cross-measure boreholes are commonly drilled in floor drainage roadways before longwall mining operations for regional gas predrainage. Notably, optimized borehole sealing techniques have become a key factor in improving sealing quality and enhancing the overall effectiveness of methane mitigation [7,8,9,10,11]. Recent studies have employed numerical simulation tools such as COMSOL Multiphysics to model gas migration under coupled mechanical-seepage fields. However, most of these studies focus on roof boreholes or assume homogeneous rock properties, neglecting anisotropic permeability, fracture evolution processes, or parameter sensitivity analysis. Importantly, there remains a lack of targeted research on floor borehole layout under dynamic mining stress conditions. Recent advances in research on cross-measure boreholes and methane drainage further support the rationale of this study. Specifically, Hosseini et al. established a 3-D numerical framework to improve methane drainage efficiency in underground coal mines; they analyzed the optimal spacing between drainage stations and the desorption-influenced zone for borehole pattern design, examined the impact of key technical parameters on methane extraction flow rates, and proposed a hybrid ANN-GWO (Artificial Neural Network-Grey Wolf Optimizer) strategy for parameter optimization [12,13,14,15,16]. Additionally, Bagherzadeh et al. Used COMSOL Multiphysics to develop optimal borehole patterns for coal-seam methane drainage under field-measured constraints [17]. Collectively, these studies emphasize the importance of parameter sensitivity-based optimization and offer external validation approaches for our multiphysics modeling method.

Therefore, this study addresses the following scientific questions:

(1) How do mining-induced fractures quantitatively affect methane migration and borehole drainage efficiency in floor strata?

(2) How can key borehole parameters (spacing, diameter, perforation depth) be dynamically optimized in accordance with the characteristics of fracture zones?

To address these questions, we propose a COMSOL-based multiphysics model to simulate the gas drainage influence radius of cross-measure boreholes and conduct parametric optimization under real-world geological conditions.

Currently, various gas management methods have been proposed to address gas influx from the protected seam into the longwall face during protective seam mining. These include the high-level drainage roadway method [18], the high-level roof drilling method [19], the goaf buried-pipe drainage method [20], and the bottom drainage roadway combined with cross-measure boreholes method [21]. These approaches effectively manage gas during the mining of lower protective seams or long-distance protective seams. However, in the case of close-distance upper protective seam mining, the development of interlayer fissure channels facilitates the influx of unloaded gas, leading to a larger volume of gas entering the longwall face-and thus limiting the effectiveness of the aforementioned methods. Consequently, recent years have seen proposals for using bottom-plate directional long boreholes for gas management [22,23,24]. This technology employs directional drilling to construct a borehole field within the roadway of the protected longwall face. The boreholes are arranged in a comb-like pattern within the rock strata between the upper and lower protective seams. The drainage mechanism works as follows: after the upper protective seam is mined, the stress in the coal and rock layers beneath the goaf decreases, inducing expansion and deformation that generate penetrating fractures. This process facilitates the desorption, migration, and diffusion of gas originally adsorbed in the coal and rock layers into the decompression space. At this stage, since the boreholes are located within the gas seepage channels, the negative pressure inside the boreholes extracts free gas into the pipeline. This reduces the influx of desorbed gas from the protected seam into the mining area of the protective seam, thereby lowering the risk of gas concentrations exceeding permissible limits at the longwall face and ensuring safe mining operations in the protective seam [25,26].

Numerous scholars have conducted extensive research on floor-based long directional borehole drainage technology. Liu et al. [27] developed a coupled coalbed methane (CBM) transport model incorporating the Klinkenberg effect to determine the effective drainage radius of directional long boreholes and to simulate how borehole negative pressure, diameter, and length influence this radius. Li [28] utilized high-level directional long boreholes to control methane in the upper corner of the longwall face and identified the optimal borehole placement based on key stratum theory and the "O-ring" theory. Field tests demonstrated that high-level directional long boreholes significantly outperform conventional high-level boreholes in drainage efficiency, effectively reducing methane concentrations in the upper corner. Xu et al. [29] used FLAC3D software to model coal seam gas drainage and identified optimal layer positions for high-level directional boreholes based on simulation results. During field implementation, secondary reaming technology was employed to improve drainage efficiency. Their analysis showed that as the longwall face advanced, gas-conducting fractures developed, and key strata fractured-leading to a gradual increase in methane flow rates. However, as the goaf compacted and fractures closed, methane flow rates decreased rapidly. Jamalan et al. [30] established a pore-fracture dual-medium system for coalbed methane (CBM) extraction based on a three-dimensional numerical model. Results indicated that the number, aperture, and layout of boreholes significantly influence the evolution of the pressure field and extraction efficiency: increasing borehole aperture or count accelerates initial pressure decay, while gas flow at later stages is primarily governed by diffusion from the matrix into fractures. This study provides a theoretical basis for optimizing CBM well network design. Tanguturi and Balusu [31] elucidated the fundamental mechanisms of gas migration in goafs through numerical simulations and experimental investigations of gas displacement processes in longwall mining goafs. Their findings reveal that gas flow in goafs is jointly affected by mining-induced subsidence, ventilation negative pressure, and fracture permeability-exhibiting heterogeneous migration characteristics both vertically and horizontally. Results further demonstrate that the efficiency of air and methane mixing and displacement in goafs depends heavily on ventilation conditions and methane source distribution, offering a theoretical foundation for optimizing ventilation and methane extraction systems. Hosseini, Madani, and Shahriar [32] conducted a numerical simulation of toxic gas diffusion (using sarin gas as a case study) in underground stations based on computational fluid dynamics (CFD). Their results indicate that gas dispersion is significantly influenced by ventilation system operation, spatial layout, and evacuation routes. Different ventilation schemes produce marked differences in the concentration distribution and dissipation rate of harmful gases. The study proposes optimized ventilation strategies and emergency control measures, providing theoretical guidance for gas dispersion safety management and disaster response in underground spaces. Based on previous studies [33,34,35], the coal-rock seam in the floor can be divided into a floor-heave fracture zone and a bottom-bulking deformation zone. Unlike the roof strata-where fracture development is strongly affected by mining height-fracture evolution in the floor strata shows low sensitivity to the mining height of the protective seam. To address the challenges of designing drainage schemes at the No. 4 seam working face of the 2130 Coal Mine, Guanghong [36] proposed a predrainage scheme using floor-penetrating comb-shaped directional long boreholes. Compared to roadway-based cross-measure boreholes, this scheme shortened construction time by 33.3% and reduced costs by 82.8%. Wang et al. [37] investigated the application of this floor-penetrating directional borehole technology in high-gas coal mines in China, highlighting its effectiveness and current challenges. Their findings emphasized that this technology offers significant advantages in methane control and emission reduction, including a high proportion of boreholes penetrating coal seams, superior drainage efficiency, and lower downtime costs. Successful applications in high-gas mines such as Daning and Baijigou have resulted in substantial improvements in gas drainage rates and reductions in methane concentrations within mine ventilation systems.

In conclusion, the current application of cross-measure directional long boreholes mainly involves arranging high-level directional boreholes in the fracture zone of the roof to control gas in the upper corner of the working face. However, studies on the use of floor-based directional long boreholes for intercepting and extracting gas from lower adjacent seams during the mining of closely spaced coal seam groups are limited. Presently, research on floor directional long boreholes is primarily based on field tests, where the selection of borehole target layers and parameters relies heavily on field experience. Notably, there has been no systematic optimization of borehole layout and parameters considering the stress evolution and permeability distribution of coal and rock strata under mining conditions. Given the importance of gas disaster prevention for safe and sustainable coal mining, this study employs COMSOL Multiphysics (a multifield coupling software) to systematically simulate and optimize borehole parameters for the 8237 and 8235 longwall faces. These faces are located in the main mining area of Qidong Coal Mine, characterized by typical interlayer gas enrichment and complex fracture structures-representing various complex geological conditions such as high gas content and high gas pressure. The primary gas sources for these faces are methane from the lower adjacent No. 9 coal seam and gas from the seam itself, both requiring targeted drainage measures [37,38,39,40,41]. This research aims to optimize floor strata gas drainage technology and cross-measure borehole parameters, providing a scientific basis for gas control in complex geological settings and offering valuable theoretical guidance and practical implications for the design and implementation of coal mine gas drainage strategies.

2. Numerical Simulation Study on Optimization of Methane Drainage via Floor Directional Boreholes

2.1. Numerical Simulation of the Numerical Solution Process

In this study, COMSOL Multiphysics is used to perform numerical simulations to optimize floor directional borehole drainage; the solution workflow is illustrated in Figure 1.

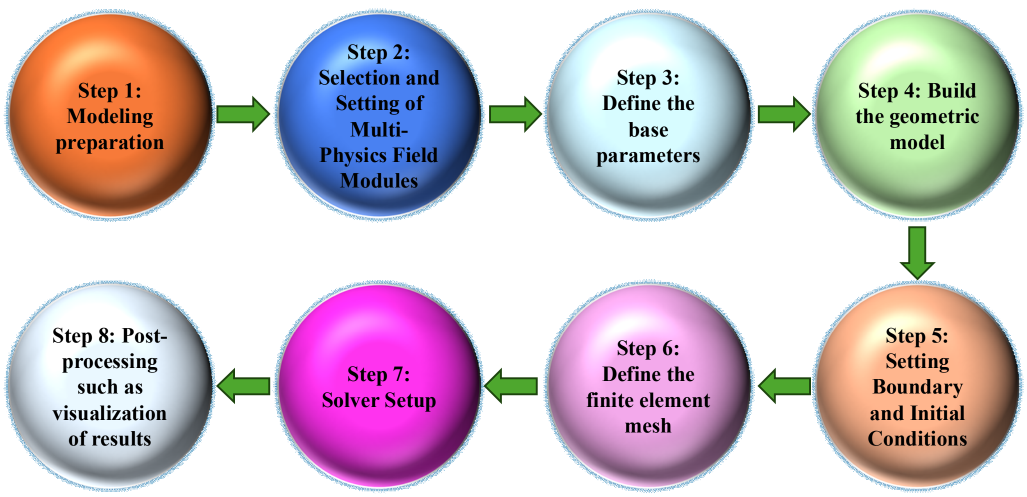

Figure 1 Numerical Solution Process

In this simulation, the following physics interfaces in COMSOL Multiphysics are employed: the Solid Mechanics (solid) interface, which models the stress-strain evolution of the coal-rock mass; the Darcy's Law (dl) interface, which describes porous-media gas flow in the coal seam; and the Transport of Diluted Species (tds) interface, which models Fickian diffusion, as well as concentration changes and mass exchange in the coal matrix driven by Langmuir adsorption-desorption. The solid and fluid fields are bidirectionally coupled via the Poroelasticity module (with Biot coefficient α): pore pressure is introduced into the solid equilibrium equation as a body force, while volumetric strain feeds back into the flow equation as a source term-this coupling mechanism is consistent with the coupled system described in Equations 10-17. The geometric model adopts a 2D plane strain configuration with triangular mesh elements. For boundary conditions: vertical in-situ stress is applied at the top boundary; roller supports are imposed on the side boundaries; the bottom boundary is fixed. For the seepage domain: zero-flux boundary conditions are set at the top and bottom boundaries; a prescribed vacuum (i.e., negative pressure) is applied at the borehole boundary.

The first type of boundary condition in this simulation is the stress boundary condition (denoted as S_σ), which is determined by the surface forces acting on the coal mass boundary. This boundary condition defines the relationship between the stress components and the surface force components on the surface force-applied boundary; it can be specified as a constant value or expressed as a function of time. Assuming the surface force components acting on the boundary along the x, y, and z directions are f_x, f_y, and f_z, respectively, and the direction cosines of the boundary's outward normal relative to the positive x, y, and z axes are l, m, and n, respectively, the stress boundary condition can be expressed as shown in Equations 1-3.

$$l\sigma_x + m\tau_{xy} + n_{xy} = f_x \quad (1)$$

$$l\tau_{xy} + m\sigma_y + n\tau_{yz} = f_y \quad (2)$$

$$l\sigma_x + m\tau_{yz} + n\sigma_x = f_z \quad (3)$$

The second type of boundary condition in this simulation is the displacement boundary condition (denoted as Su), which is defined by the prescribed displacement at the coal mass boundary. When the displacement at the boundary is prescribed, the displacement components of the coal mass at the boundary equal the given displacement values, as shown in Equation 5 below.

$$u_i = \overline{u_i};\quad v_i = \overline{v_i};\quad w_i = \overline{w_i} \quad (4)$$

where are:

u_i - the displacement components of the coal mass at the boundary along the x directions,

v_i - the displacement components of the coal mass at the boundary along the y directions,

w_i - the displacement components of the coal mass at the boundary along the z directions,

$\overline{u_i}$ - the constrained displacement components determined at the x boundary,

$\overline{v_i}$ - the constrained displacement components determined at the y boundary,

$\overline{w_i}$- the constrained displacement components determined at the z boundary,

The third type of boundary condition in this simulation is the mixed boundary condition S, which is characterized by a combination of displacement boundary conditions and stress boundary conditions. These two types of boundary conditions can be prescribed separately on different regions of the coal mass boundary, or along different directions within the same boundary region. This condition is expressed in Equation 5 below:

$$S = S_\sigma + S_u \quad (5)$$

Stress field initial condition: the magnitude of the initial displacement of the coal body when t = 0, i.e., $u_{t=0} = \overline{u}$.

Prior to conducting the numerical simulation, the following basic assumptions are established for the model to simplify computational complexity while ensuring the reliability of results:

(1) The coal mass is treated as an elastoplastic material.

(2) The initial pore structure of the coal mass is uniformly distributed, with the influence of primary fractures neglected. The initial permeability of the coal mass is isotropic and homogeneous.

(3) Methane seepage in fractures follows Darcy's Law, while methane flow in matrix pores adheres to Fickian diffusion.

(4) The methane drainage process is assumed to be isothermal, with heat absorption and release during methane adsorption-desorption processes neglected.

(5) Methane is treated as an ideal gas, and its density is calculated using the equation: $P_g = \frac{pM}{RT}$,

Where are:

P - methane pressure (MPa),

M - the molar mass of methane (g/mol),

R - the universal gas constant (J/(mol·K)),

T - absolute temperature (K) (consistent with the isothermal assumption in (4)).

Rock strata parameters in the model are set based on field test data from Qidong Coal Mine. The heterogeneity of rock strata is characterized by assigning different permeability and porosity (ϕ) values to different regions; meanwhile, fissure distribution is represented by adjusting local permeability to enhance the simulated gas conductivity of fractures in the target area. Although the microscopic fracture network structure is not fully captured, the main geological inhomogeneities have been reasonably simulated through parameter differentiation.

2.2. Coal Mass Deformation-Gas Flow Coupling Modeling

Flow inside the drainage borehole follows the Navier-Stokes framework; however, in the present study, since our focus is on analyzing seam-scale poroelastic Darcy flow and parameter sensitivities, borehole hydraulics are simplified as an equivalent boundary condition-a prescribed negative pressure at the borehole wall or inlet, with in-pipe losses lumped into this boundary treatment. Methane migration in the coal-rock mass is modeled as continuum porous-media flow via Darcy's law, while Fick-type diffusion and Langmuir adsorption-desorption are used to describe mass exchange in the coal matrix. The fluid mass balance equation is coupled with solid deformation through the Biot coefficient and adsorption-induced strain; the complete set of coupled equations used herein is provided in Equations 10-17. Methane is treated as an ideal gas, with density calculated in situ as ρ_g = $PM/(RT)$. Given the small deviation from real-gas behavior over our study range, we did not introduce an additional real-gas equation of state; if needed, a compressibility factor Z can be incorporated without changing the coupling structure.

(1) Coal mass deformation governing equation

Under the assumption of negligible inertia, the equilibrium equation for the coal mass is given by Equation 6:

$$\sigma_{ij} + f_i = 0 \quad (i=1, 2, 3; j=1, 2, 3) \tag{6}$$

Where are:

σ_{ij} - the stress tensor of the coal mass (N/m^3),

f_i - the body force vector (N/m^3).

The relationship between the strain and displacement components is expressed by the geometric equation (Equation 7).

$$\varepsilon_{ij} = \frac{1}{2}(u_{i,j} + u_{ji}) \tag{7}$$

Where are:

ε_{ij} -the strain tensor,

$u_{i,j}$, u_{ji} - the displacement component.

Assuming that coal swelling due to gas adsorption is isotropic [41,42], the adsorption-induced strain can be described by a Langmuir-type equation (Equation 8).

$$\varepsilon_s = \frac{\varepsilon_L p}{P_L + p} \tag{8}$$

Where are:

ε_s - the adsorption-induced strain;

ε_L - the Langmuir volume strain constant;

P_L - the Langmuir pressure constant (Pa),

P - the gas pressure (Pa).

The constitutive equation for the coal mass considering adsorption is given by Equation 9:

$$\varepsilon_{ij} = \frac{1}{2G}\sigma_{ij} - \left(\frac{1}{6G} - \frac{1}{9K}\right)\sigma_{kk}\delta_{ij} + \frac{\alpha}{3K}p\delta_{ij} + \frac{\varepsilon_s}{3}\delta_{ij} \tag{9}$$

Where are:

G - the shear modulus (Pa);

δ_{ij} - the Kronecker symbol;

a - Biot's constant, and $a=1-1-K/K_s$,

K_s - the bulk modulus of the coal body skeleton (Pa),

K - the bulk modulus of the coal (Pa);

σ_{kk} - the stress tensor form of the coal body (Pa).

Although Equation 9 adopts a linear-elastic assumption, the strain-softening behaviour and anisotropic permeability evolution of fractured coal are equivalently represented through the stress-dependent fracture permeability model and spatially oriented permeability tensor Table 1.

The control equation of coal body deformation can be obtained by associating Equations 6-9 as Equation 10:

$$Gu_{i,kk} + \frac{G}{1-2v}u_{k,ki} - \alpha p_{,i} - K\frac{\varepsilon_L P_L}{(P_L + p)^2}p_{,i} + f_{,i} = 0 \tag{10}$$

Where are:

$u_{i,kk}$, $u_{k,ki}$ - the displacement tensor forms;

v - the Poisson's ratio of the coal; and the symbols in the low-er right corner of $p_{,i}$ are the derivation symbols expressed in tensor form in mechanics.

(2) Gas flow control equation

The dynamic equilibrium state of the gas during flow in the coal body can be expressed as Equation 11:

$$\frac{\partial m}{\partial t} + \nabla \cdot (\rho_g \vec{q}_g) = Q_s \tag{11}$$

Where are:

ρ_g - the density of gas (kg/m^3);

t -time (s);

m - the mass of gas contained in the unit volume of coal body (kg/m^3);

q_g - the seepage velocity of gas (m/s),

"⟶" - indicates that the seepage velocity is a vector; ,

Q_s - the source of mass (kg/m^3), $Q_s = (c - c_p)\tau$;

c and c_p - the content of free gas and adsorbed gas in the coal seam (kg/m^3);

τ - the resolved diffusion coefficient of gas (s$^{-1)}$;

∇ - the divergence of the gas mass flux density, representing the rate of gas mass inflow or outflow per unit volume within the coal matrix. (kg/(m^3·s)), The gas density can be found using the following Equation 12:

$$\rho = \frac{M}{RT}p \quad (12)$$

Where are:

M - the molecular mass of methane (16 g/mol);

P - the gas pressure (Pa);

R - the gas molar constant (J/(mol·K));

T - the Kelvin temperature (K).

The model fully considers the adsorption and desorption behaviors of gas in the coal body, and constructs the adsorption-desorption kinetic expressions based on Langmuir theory. Equations. 13 to 16 reflect the effect of desorption rate on the change of gas pressure. Since the permeability of the coal body is much less than 1, the total mass of gas per unit volume of coal body can be expressed as Equation 13:

$$m = m_1 + m_2 = \rho_g \phi + \rho_{ga}\rho_c \frac{V_L}{P_L + p}p \quad (13)$$

Where are:

ρ_g - the density of free gas (kg/m^3);

ρ_{ga} - the density of adsorbed gas (kg/m^3);

ϕ - the porosity;

ρ_c - the density of the coal body (kg/m^3);

V_L - the Langmuir volume constant (MPa);

P - the pressure of the gas in the coal body (Pa);

P_L - the Langmuir pressure constant (MPa).

Derivation of Equation 13 yields:

$$\frac{\partial m}{\partial t} = \frac{M_g p}{RT}\frac{\partial \phi}{\partial t} + \frac{M_g \phi}{RT}\frac{\partial p}{\partial t} + \rho_c \frac{M_g}{RT}\frac{V_L p}{P_L + p}\frac{\partial p}{\partial t} \quad (14)$$

The seepage of gas in a coal seam can be expressed as Equation 15 by using Darcy's law:

$$\vec{q}_g = -\frac{k}{\mu}\nabla p \quad (15)$$

Where are:

k - the permeability of the coal body (m^2);

μ - the dynamic viscosity coefficient of the gas (Pa·s);

∇p - the gas pressure difference in the coal body (Pa).

Substituting Equations 14-15 into Equation 12 yields the control equation for gas flow in the coal seam as Equation 16:

$$p\frac{\partial \phi}{\partial t} + \left(\phi + \frac{\rho_c V_L p}{P_L + p}\right)\frac{\partial p}{\partial t} - \nabla \cdot \left(\frac{k}{\mu}p\nabla p\right) = Q_S \quad (16)$$

The coupled coal body deformation-gas flow gas-solid coupling model is obtained by combining Equation 10 and Equation 16, as in Equation 17:

$$\begin{cases} Gu_{i,kk} + \dfrac{G}{1-2v}u_{k,ki} - \alpha p_{,i} - K\dfrac{\varepsilon_L P_L}{(P_L + p)^2}p_{,i} + f_{,i} = 0 \\ p\dfrac{\partial \phi}{\partial t} + \left(\phi + \dfrac{\rho_c V_L p}{P_L + p}\right)\dfrac{\partial p}{\partial t} - \nabla \cdot \left(\dfrac{k}{\mu}p\nabla p\right) = Q_S \end{cases} \quad (17)$$

The "velocity" herein denotes the Darcy velocity (specific discharge), obtained from Darcy's law; its magnitude and direction are governed by the permeability-viscosity ratio and the pressure gradient, respectively. The pore velocity can be recovered as $v=q/\phi$ if needed.

2.3. Geometric Modeling of the Coal Seam System

The interbedded rock layer between the 8_2nd and 9th coal seams was selected as the research object, and a two-dimensional (2D) plane-strain model was established, as illustrated in Figure 2. Rock formation parameters in the model were set based on field test data from Qidong Coal Mine; heterogeneity of the rock formation was characterized by assigning different permeability and porosity values to various regions, while fissure distribution was represented by adjusting local permeability to enhance the simulated gas inflow capacity of fissures in the target region. Although the microscopic fracture network structure was not fully captured, key geological inhomogeneities were reasonably simulated through parameter differentiation.

To simplify the model, the computational domain was designed with a length of 20 m and a height of 12.2 m, with directional boreholes arranged in the central part of the interbedded rock layer. Table 1 presents the basic parameters of the rock formation used for the simulation; the initial permeability listed in Table 1 was derived from triaxial permeability field measurements at Qidong Coal Mine (2023).

Boundary conditions were defined as follows:

1. Stress field: The upper boundary of the rock layer was subjected to a stress load with a magnitude equal to the in-situ vertical stress of the rock formation; the left and right boundaries were set as roller supports; the lower boundary was constrained with fixed conditions (i.e., the displacement of the lower boundary of each layer was set to zero).

2. Seepage field: The initial methane pressure in the rock layer was set to 1.5 MPa; methane flows only within the interbedded rock layer and cannot migrate out of the upper and lower rock slabs (i.e., the upper and lower boundaries of the simulated domain were set as zero-flux boundaries); the negative pressure for borehole drainage was set to 15 kPa.

Although the model employed in this study is two-dimensional and restricted to a relatively small domain, it is designed to capture lateral methane migration around boreholes and enable efficient parametric analysis. The research focus is on identifying trends and sensitivities in drainage performance under different borehole parameters, rather than reproducing full-scale mining site geometries. To mitigate potential boundary effects, the observation area was limited to the central region of the model-sufficiently far from the domain edges. This modeling strategy has been validated in prior studies and remains effective for evaluating localized flow behavior. Future work will extend this framework to full three-dimensional (3D) models to improve spatial resolution and incorporate vertical fracture connectivity.

To balance computational accuracy and efficiency, the 2D plane-strain domain was discretized using triangular elements, with local mesh refinement applied near boreholes and high-gradient regions. Table 1 summarizes the key mesh metrics (with quality evaluated using COMSOL's default criteria).

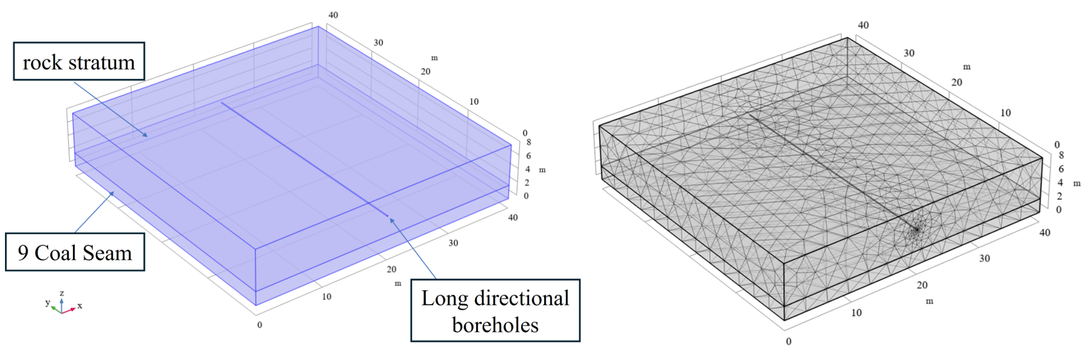

Figure2. Borehole model after grid delineation

Table 1. Simulation parameter settings and mesh statistics (2-D)

name	value	unit
Floor porosity (ϕ)	0.02	-
Langmuir volume (VL)	0.033	m^3/kg
Fracture spacing	0.5	m
Poisson's ratio	0.19	-
Langmuir pressure constant	0.716	MPa
Initial gas pressure	1.5	MPa
Initial permeability	1.5×10^{-17}	m^2
Gas desorption diffusion coefficient	1	s^{-1}
Drainage negative pressure	15	kPa
Methane molecular weight	16	g/mol
Gas dynamic viscosity	2×10^{-5}	Pa·s
Universal gas constant	22.4	L/mol
Temperature	293	K
Mesh vertices	27,184	-
Tetrahedra	- (2-D)	-
Triangles	25,036	-
Edge elements	1,982	-
Vertex elements	148	-
Number of elements	25,036	-
Minimum element quality	0.48	-
Average element quality	0.76	-
Element volume ratio (max/min)[1]	295	-
Mesh volume (2-D area)[2]	244	m^2

3 Optimization of Borehole Parameters Based on Numerical Simulation Models

3.1. Gas Drainage Behaviour under Varying Longwall Advance Distances

As the longwall face advances, spatial variations in floor decompression and fracture penetration become apparent. Specifically, directional boreholes gradually enter the active gas drainage zone, while the surrounding fracture network expands correspondingly. The drainage performance under different face advance distances is illustrated in Figure 3. When the longwall face advances 50 m, the floor decompression range is limited, and floor fractures only form below the caving zone. As a result, the borehole tip (deep end) exhibits a better drainage effect than the borehole inlet (shallow end). Notably, when the advance distance reaches 100 m, 150 m, and 200 m, the length of directional boreholes penetrating the caving zone increases; this expands the contact area between penetrating fractures and the boreholes, leading to a gradual extension of the drainage range. This trend can be attributed to stress redistribution and fracture evolution induced by longwall face advancement. As overburden pressure is released, the floor strata undergo tensile and shear failure, which generates new fractures or extends existing ones. These fractures enhance the permeability of the coal-rock mass, thereby improving pathways for gas desorption and migration. Consequently, with increasing advance distance, the contact area between directional boreholes and gas migration channels expands-this enlarges the effective drainage radius and significantly enhances overall drainage performance. Figure 3 Drainage effectiveness of boreholes at varying longwall advance distances, since Darcy velocity is driven by the pressure gradient, its temporal evolution mirrors the evolution of the pressure field: At early stages, a distinct high-pressure-gradient zone forms near the borehole, generating a "high velocity in near-borehole regions, low velocity in far-field regions" pattern that extends along higher-permeability flow pathways. Over time, the overall pressure differential diminishes, leading to a corresponding decrease in velocity magnitude-nevertheless, the dominant flow channels remain oriented toward the borehole; As the pressure field approaches quasi-equilibrium, the high-velocity region shrinks, reflecting stable preferential flow pathways and a gradual reduction in flow magnitude. The evolutionary trend aligns with the temporal changes in pressure contours.

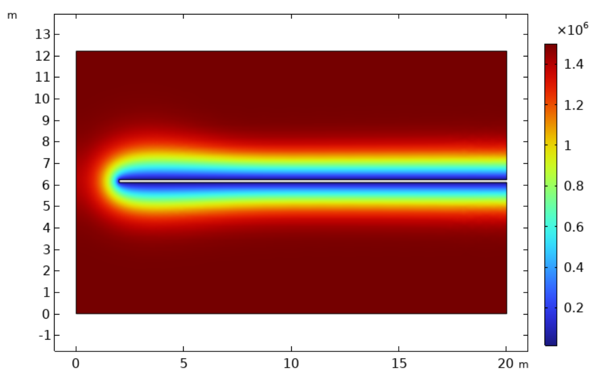

(a) Advancement of the longwall face by 50 m

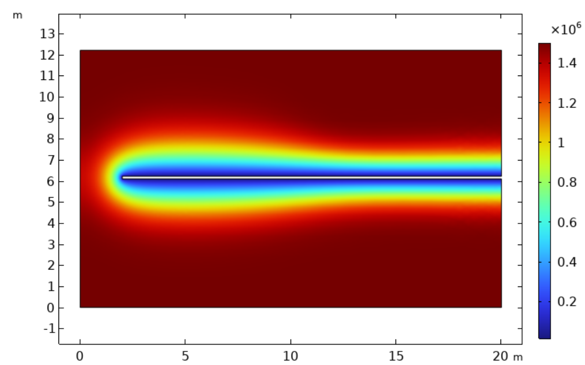

(b) Advancement of the longwall face by 100 m

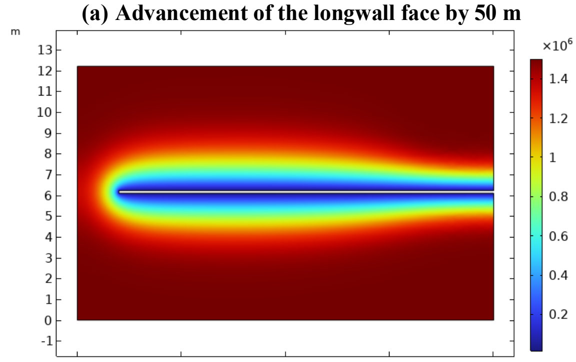

(c) Advancement of the longwall face by 150 m

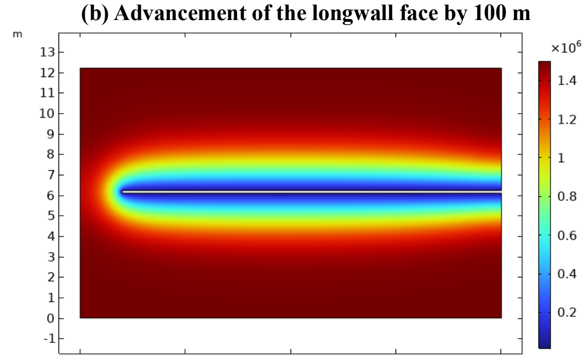

(d) Advancement of the longwall face by 200 m

Figure3. Drainage effectiveness of boreholes at varying longwall advance distances

Since Darcy velocity is driven by the pressure gradient, its temporal evolution mirrors the evolution of the pressure field:

1. At early stages, a distinct high-pressure-gradient zone forms near the borehole, generating a "high velocity in near-borehole regions, low velocity in far-field regions" pattern that extends along higher-permeability flow pathways;

2. Over time, the overall pressure differential diminishes, leading to a corresponding decrease in velocity magnitude. nevertheless, the dominant flow channels remain oriented toward the borehole;

3. As the pressure field approaches quasi-equilibrium, the high-velocity region shrinks, reflecting stable preferential flow pathways and a gradual reduction in flow magnitude.

This evolutionary trend aligns with the temporal changes in pressure contours.

3.2. Optimization of Borehole Placement Horizon

After mining-induced pressure release, the coal seam floor heaves upward from the abutment areas toward the center of the goaf, forming a fracture zone. Vertical permeability varies sharply in space, leading to uneven methane accumulation. Vertical fractures intersect with bedding-plane partings-this not only enhances the bulk permeability of the rock mass but also enables full methane desorption and migration toward the longwall face. If methane concentrations exceed statutory safety limits, this poses a gas outburst risk.

The drainage performance of floor directional boreholes depends on the permeability of the host rock; meanwhile, the vertical distance from the coal seam floor determines the length of the effective drainage interval. A lower borehole placement (closer to the goaf) lengthens the productive drainage section but may position the borehole in a low-permeability horizon, making careful horizon selection critical [43,44]. Figure 4 compares the drainage effects of three discrete placement scenarios (3 m, 6 m, and 9 m below the coal seam floor); continuous gradient analysis confirms that the optimal placement range is 3-5 m below the seam floor.

Figure 4 illustrates the borehole layout scheme adopted in this simulation. To examine the effect of vertical position on drainage performance, directional boreholes were placed at three vertical intervals: 3 m, 6 m, and 9 m above the 9th coal seam roof. After the longwall face advanced 100 m, the simulation results (Figure 4) reveal that the effective drainage radius and associated drainage efficiency exhibit a progressive reduction as the borehole position shifts from 3 m to 9 m above the 9th coal seam roof.

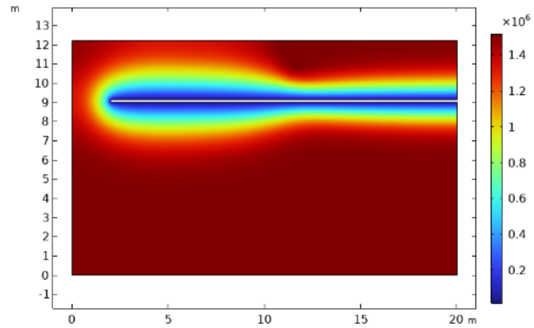

(a) 9m from the 9-coal roof

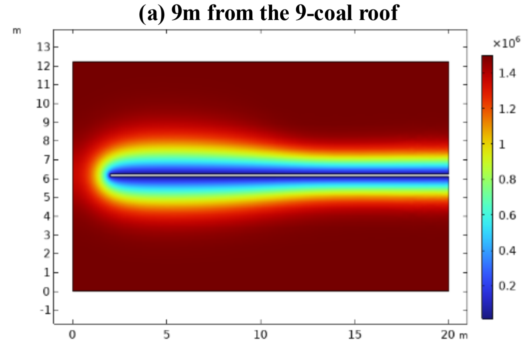

(b) 6m from the 9-coal roof

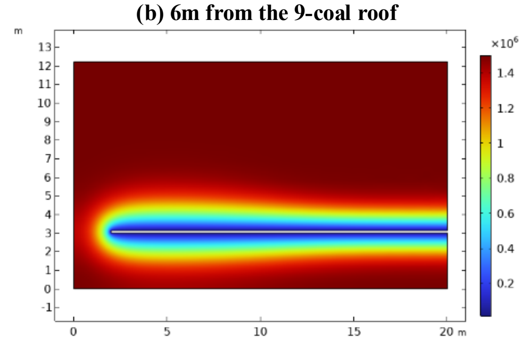

(c) 3m from the 9-coal roof

Figure4. Layout of boreholes during simulation

This trend can be attributed to the decreasing degree of floor decompression with increasing distance from the 8_2nd coal seam mining area. Greater distance from the mining disturbance leads to fewer newly generated fractures and reduced fracture connectivity in the host rock-both factors constrain methane migration toward the boreholes. Consequently, floor directional boreholes should be positioned as close as practically feasible to the 8_2nd coal seam floor; ideally, this corresponds to the interval of 3-5 m above the 9th coal seam roof (matching the optimal vertical range identified in Section 3.2).

3.3. Optimization of Directional Borehole Parameters

Using the above parameter set and the effective drainage radius criterion, single-borehole simulations were conducted for 90, 180, and 270 days-this accounts for the varying drainage characteristics of different coal seams at Qidong Coal Mine. Figure 5(a) presents gas pressure contours for the minimum-permeability scenario, while Figure 5(b) shows the corresponding regional pressure profiles. The contours reveal that the pressure reduction halo around a single borehole expands steadily with both drainage duration and longwall face advance.

These results indicate that, under the coal seam conditions at Qidong Coal Mine, directional boreholes can be constructed easily, and directional borehole drainage can significantly reduce coal seam gas pressure within a short period. As shown in Figure 5(a-c), the gas pressure distribution changes significantly as drainage time increases from 90 to 270 days: pressure isolines gradually expand outward from the borehole center, reflecting an increase in the effective radius of influence over time. This behavior is attributed to enhanced gas migration capacity and expanded permeability pathways, driven by continuous gas desorption and coal matrix shrinkage. Longer drainage duration leads to greater connectivity of the fracture network, which facilitates gas seepage and expands the effective drainage area.

However, in actual pre-drainage operations, the reduction in coal seam gas content causes coal matrix contraction, which in turn induces dynamic changes in coal seam permeability. Additionally, considering the influence of borehole trajectory curvature, gas flow includes not only radial flow from the coal-rock mass toward the borehole but also flow within the borehole itself.

Based on the previously determined single-borehole effective drainage radius (6-8 m), a competitive drainage factor of 0.85 was applied to account for multi-borehole interference. The resulting optimal directional borehole spacing is 10-14 m, which aligns with the on-site recommended spacing of 12-16 m for Qidong Coal Mine.

Based on the strike length of the longwall face, a minimum of four directional borehole sites should be arranged, with an interval of approximately 200 m between adjacent sites. Each site requires at least five directional boreholes, resulting in a total of no fewer than 20 boreholes per longwall face.

For borehole construction parameters: the collar (drilling initiation section) should be oriented at an angle of 35°-45° relative to the site roadway, with an initial azimuth of 135°-145°; the borehole termination section should be parallel to the longwall face, with a final azimuth of approximately 100°.

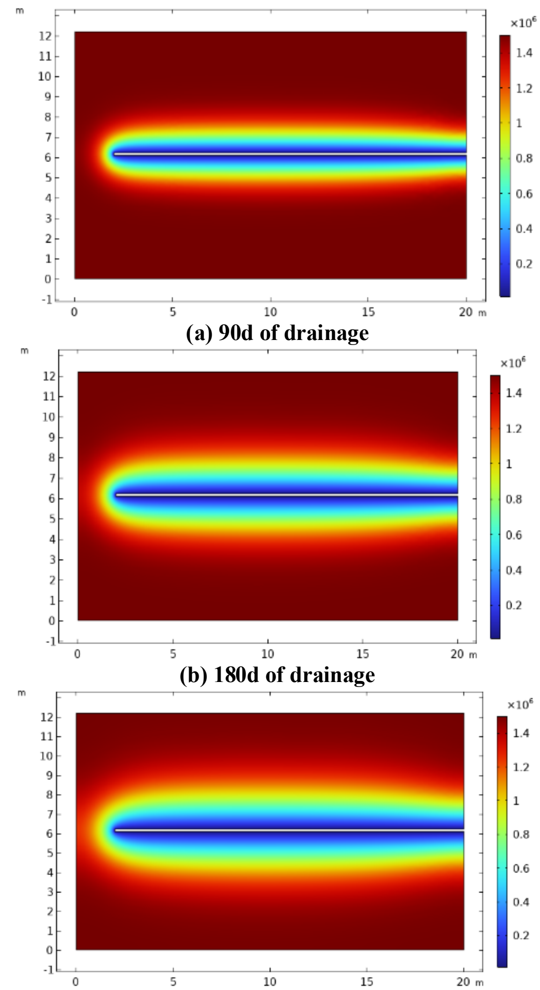

Figure5. Numerical simulation results of gas pressure distribution around a single borehole after (a) 90 days, (b) 180 days, and (c) 270 days of drainage

3.4. Optimization of Borehole Diameter

Increasing the borehole diameter expands the borehole wall surface area, which in turn enhances gas capture capacity and improves overall drainage efficiency. From a construction perspective, however, larger diameters increase drilling difficulty, reduce drilling advance rates, and may lead to borehole collapse or instability (even borehole abandonment in severe cases)-ultimately driving up construction costs.

To determine the optimal borehole diameter, we simulated three common field-used borehole diameters (76 mm, 120 mm, and 153 mm), keeping all other parameters constant to isolate the effect of diameter on drainage performance. The model assesses drainage performance over a 90-day period for boreholes constructed at the same horizon, with the simulation scenario set to a longwall face advance distance of 100 m.

Figure. 7 and 8 demonstrate that increasing the borehole diameter expands the gas-borehole wall contact area and the negative pressure low-attenuation zone, thereby extending the effective drainage radius. However, compared with the 120 mm borehole, the 153 mm borehole only yields a marginal increase in the effective drainage radius-yet incurs significantly higher drilling costs. Consequently, a borehole diameter of 120 mm is recommended whenever practically feasible.

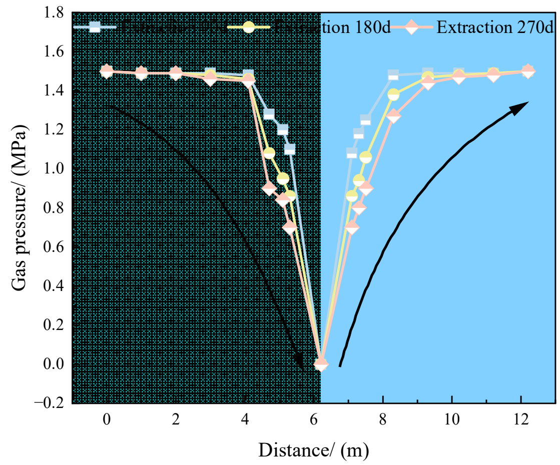

Figure6. Regional gas pressure distribution at different drainage times

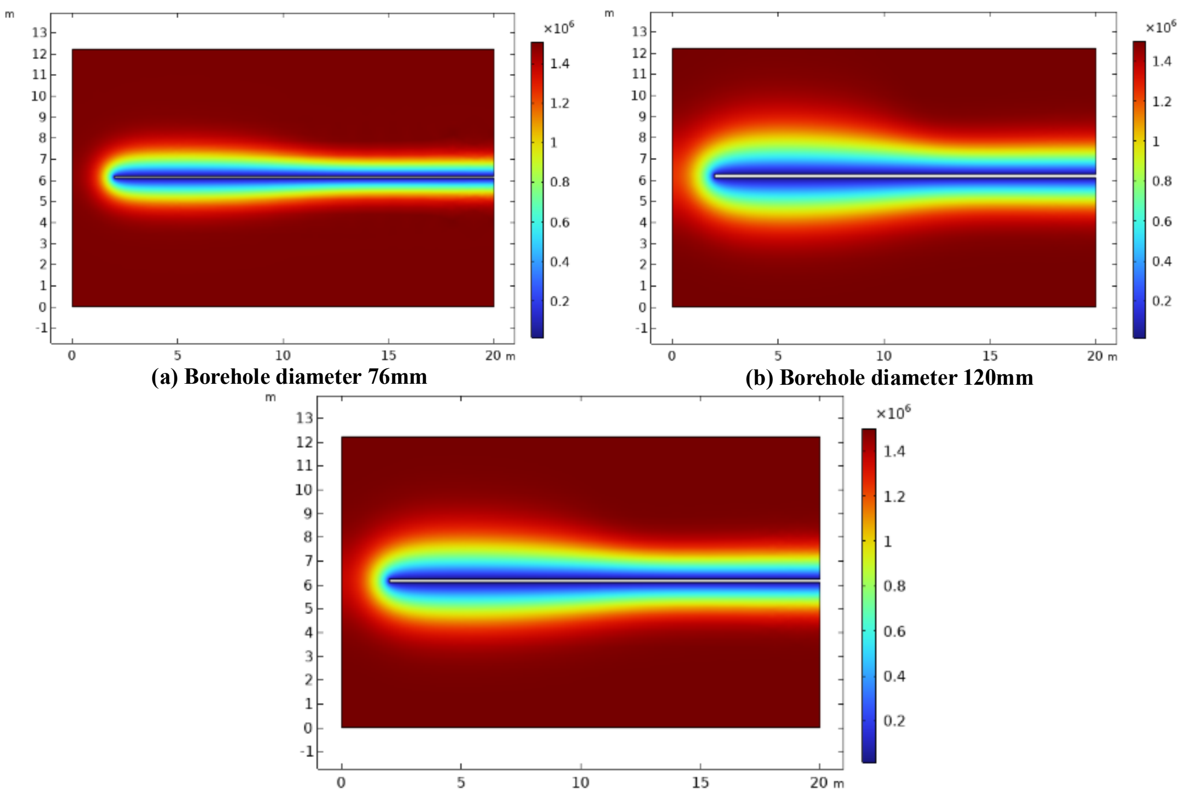

(a) Borehole diameter 76mm

(b) Borehole diameter 120mm

(c) Borehole diameter 153mm

Figure7. Numerical simulation results of the effect of drainage for 90d under different borehole diameter condition

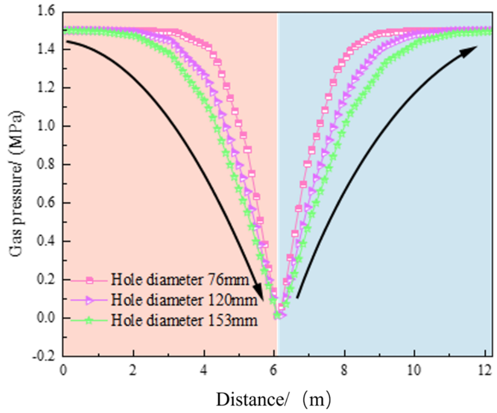

Figure8. Regional gas pressure distribution after drainage with different borehole diameters

3.5 Optimization of Borehole Length

To optimize borehole length, simulations were conducted for three effective section lengths (10 m, 14 m, and 18 m) under the scenario of a 100 m longwall face advance.

Results (Figure 9) indicate that longer effective sections not only expand the range of gas diffusion via fracture seepage but also increase the borehole's influence radius and enhance cumulative gas extraction. Based on on-site conditions at Qidong Coal Mine, the final drilling depth of boreholes should be controlled within the range of 550-650 m to ensure the effective section length meets the pre-drainage requirements.

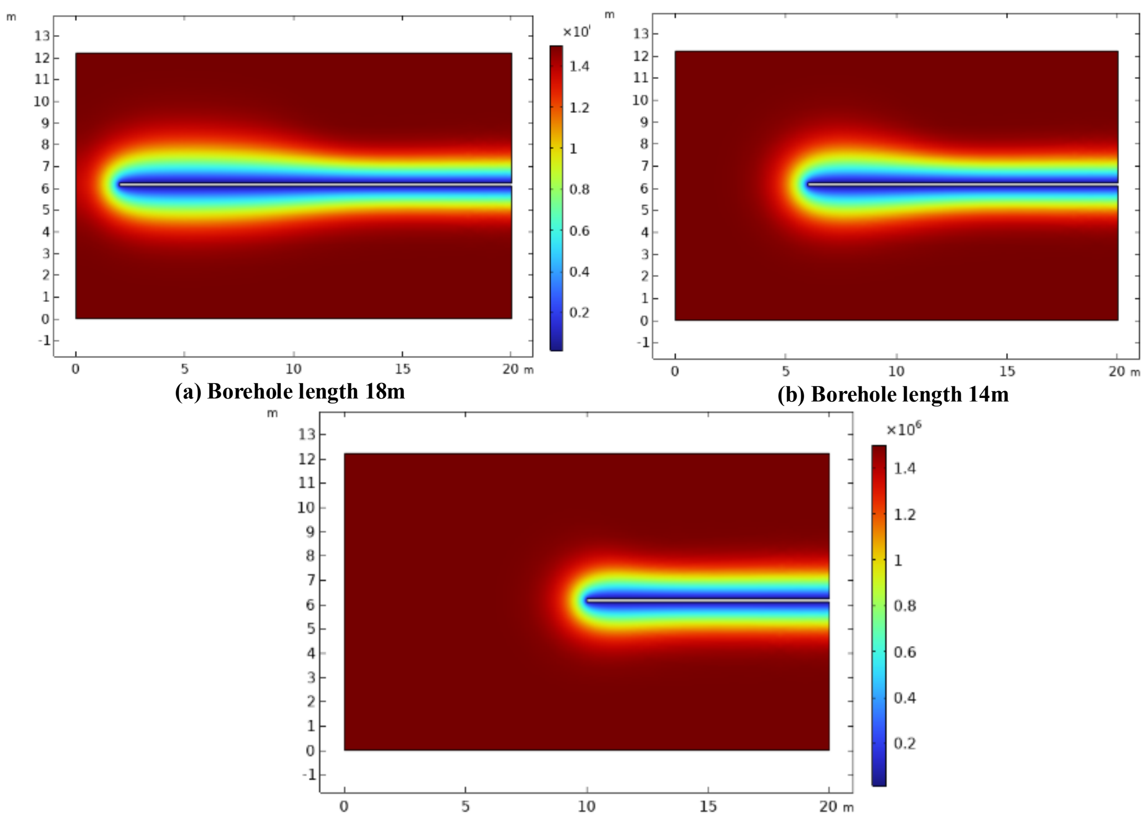

(a) Borehole length 18m **(b) Borehole length 14m**

(c) Borehole length 10m

Figure9. Numerical simulation results of drainage effect for different borehole lengths

4. Numerical Modeling of Gas Drainage for Floor Cross-Measure Boreholes

4.1. Numerical Modeling of Gas Drainage via Cross-Measure Boreholes for Parameter Optimization

In field practice, cross-measure boreholes are typically inclined at approximately 30-45° to penetrate fracture corridors from the roadway. For the 2-D model developed in this study, the productive segment (effective drainage section) is represented by its horizontal projection within a single stratigraphic layer. This simplification aims to achieve three objectives: (i) isolate the sensitivity of drainage performance to layer-specific parameters (spacing, diameter, vacuum pressure), (ii) avoid boundary artifacts caused by out-of-plane effects, and (iii) keep computational costs manageable for systematic parameter sweeps.

Notably, near-borehole flow is primarily governed by the local permeability structure and the applied vacuum pressure, rather than the borehole inclination itself. Therefore, the optimization trends for key parameters (spacing, diameter, vacuum pressure) derived from the 2-D model are applicable to inclined cross-measure boreholes in practical applications. A subsequent 3-D model-incorporating realistic borehole trajectories and multi-layer coupling-will be developed to quantify the specific effects of borehole inclination.

In this simulation, the solid-gas dynamic coupling model for low-permeability coal-rock and gas is solved using finite element analysis (FEA), involving the numerical solution of both the gas seepage field and the coal-rock deformation field. We assume that the basic parameters and stress state of the coal-rock mass and gas remain consistent along the dip and strike directions of the coal seam. Based on this assumption, a vertical profile along the borehole is established for analytical purposes. The computational geometric model is illustrated in Figure 10, and the relevant model parameters are summarized in Table 2.

The deformation behavior of the gas-containing coal-rock mass is governed by a complex three-dimensional (3D) mechanical model, which involves the coupling of gas-solid interactions between methane and the coal skeleton. This complexity results in a substantial computational workload. To improve efficiency, the model is simplified to a two-dimensional (2D) framework.

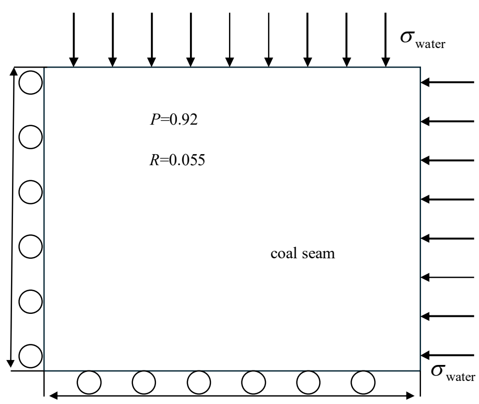

Figure10. Computational geometric model and boundary conditions

This 2D model focuses on the coupling of the gas seepage field and the planar deformation field of the coal-rock mass; due to the nonlinearity of the coupled multiphysics fields, only numerical solutions can be obtained. As the model is described by a system of partial differential equations (PDEs) representing multiphysics coupling, it can be analyzed using COMSOL Multiphysics software (via the finite element analysis method), with numerical solutions implemented through the PDE solver within the software.

Table 2. Simulation Parameter Settings

name	value	unit
9 Coal seam porosity (ϕ)	0.02	-
Langmuir volume (VL)	0.033	m^3/kg
Fracture spacing	0.05	m
Poisson's ratio	0.19	-
Langmuir pressure constant	0.716	MPa
Initial gas pressure	1.5	MPa
Initial permeability	1.5×10^{-17}	m^2
Gas desorption diffusion coefficient	1	s^{-1}
Drainage negative pressure	15	kPa
Methane molecular weight	16	g/mol
Gas dynamic viscosity	2×10^{-5}	Pa·s
Universal gas constant	22.4	L/mol
Temperature	293	K

The numerical simulation scheme was designed as follows, with a consistent 180-day duration for all gas drainage simulations to ensure comparability:

1. To investigate the effect of directional borehole drainage spacing on drainage performance, eight scenarios were tested, with spacings ranging from 10 m to 45 m at 5 m intervals (i.e., 10 m, 15 m, 20 m, ..., 45 m). The drainage negative pressure was fixed at -10 kPa for all spacing scenarios.

2. To analyze the influence of borehole diameter on gas drainage, four borehole diameters were selected for simulation: 76 mm, 94 mm, 108 mm, and 120 mm. The drainage negative pressure was also fixed at -10 kPa to isolate the diameter effect.

3. To assess the impact of drainage negative pressure on gas drainage, four pressure scenarios were tested: -10 kPa, -20 kPa, -30 kPa, and -40 kPa. No other parameters were adjusted to ensure the pressure effect was the sole variable.

4.2. Analysis of Cross-Measure Borehole Drainage Performance Under Varying Operating Conditions

4.2.1. Optimization of Directional Cross-Measure Boreholes

Figure 11 illustrates the gas pressure contours for different borehole spacings. As the borehole spacing increases, the gas pressure between adjacent boreholes rises gradually; in contrast, an appropriate spacing can reduce the seam gas pressure to the required safety level. Thus, borehole spacing is a key factor that directly determines the effectiveness of gas drainage.

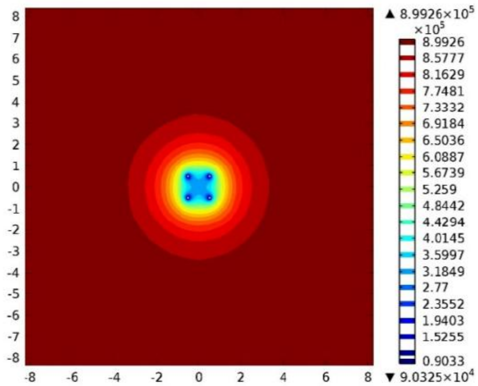

(a) 10 meters apart

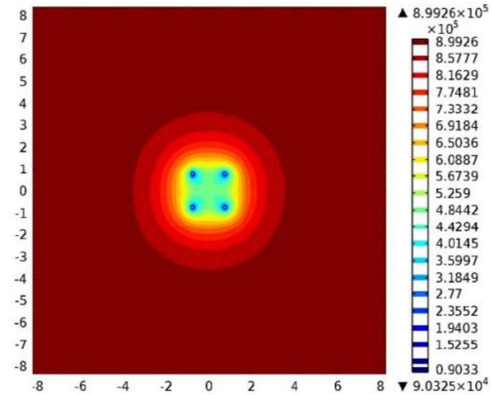

(b) 15 meters apart

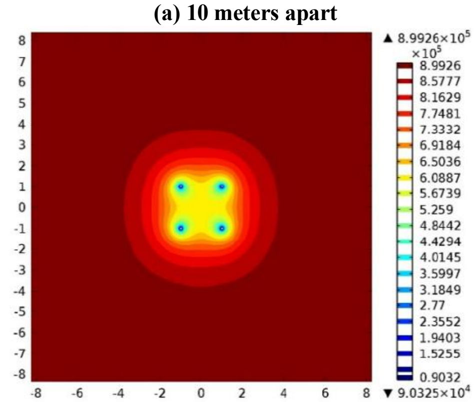

(c) 20 meters apart

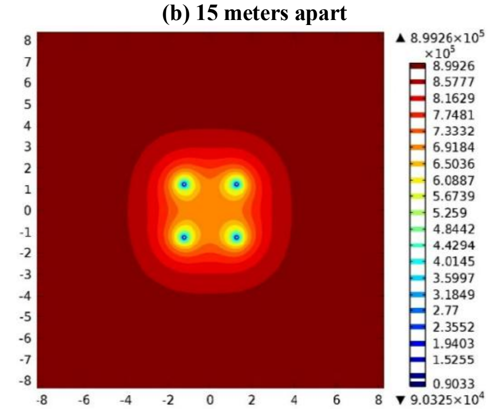

(d) 25 meters apart

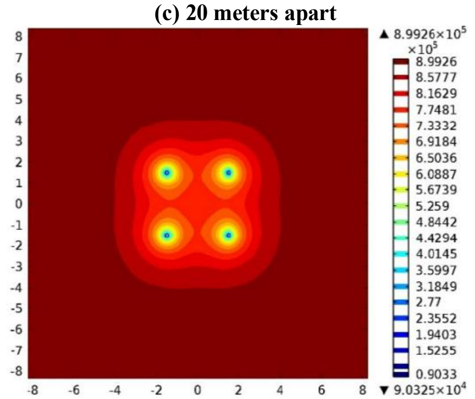

(e) 30 meters apart

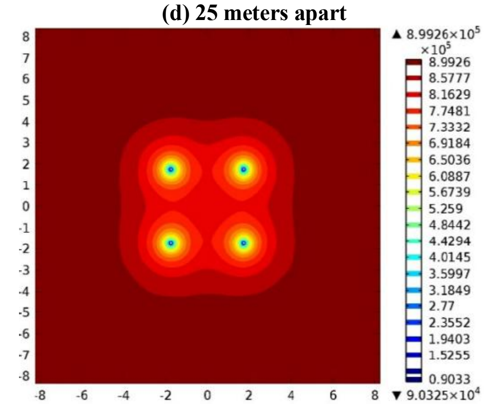

(f) 35 meters apart

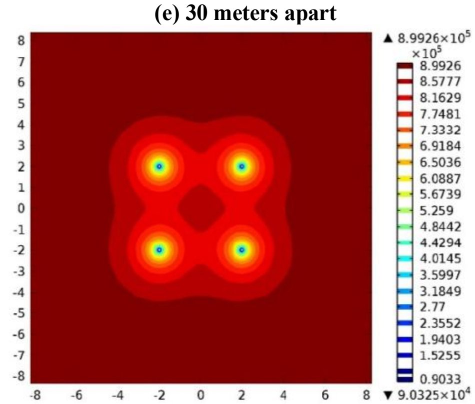

(g) 40 meters apart

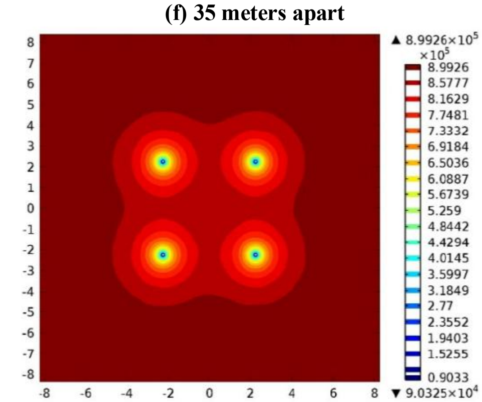

(h) 45 meters apart

Figure11. Cloud map of gas pressure distribution with different directional boreholes

To analyze the gas pressure distribution under different directional borehole spacings, the gas pressure along a horizontal line connecting the left and right endpoints of the borehole array was examined. According to the Basic Indicators for Coal Mine Gas Drainage, the gas pressure in coal seams at the outburst-risk depth should be reduced to less than 0.74 MPa, regardless of the specific burial depth of the coal seam.

As shown in Figure 12, the gas pressure at the midpoint of the borehole line increases with increasing borehole spacing, but the rate of increase gradually decreases. When the borehole spacing is 25 m, the gas pressure at the midpoint between two adjacent boreholes is reduced to below 0.74 MPa. Therefore, directional borehole spacing is a key factor influencing the effectiveness of coal seam gas drainage. Based on the numerical simulation analysis, it is recommended that the borehole spacing for the 8235longwall face of Qidong Coal Mine be set within the range of 20-25 m.

4.2.2. Optimization of Cross-Measure Borehole Diameter

Figure 13 presents the gas pressure contours for different borehole diameters. The contours indicate that borehole diameter exerts only a minor influence on the overall gas pressure distribution within the drainage zone. This observation confirms that, within the scope of the simulated diameters (76 mm-120 mm), borehole diameter is not a primary determinant of gas drainage effectiveness.

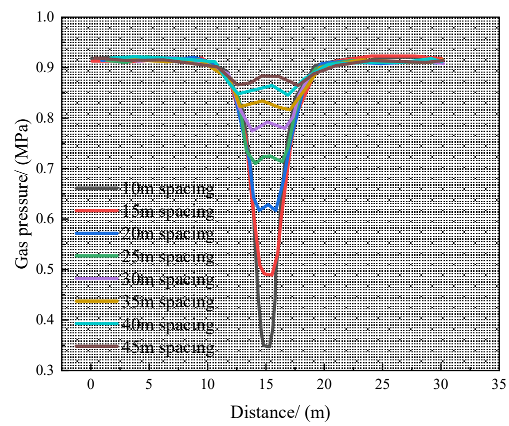

Figure12. Gas pressure distribution curves around boreholes with different drill spacing

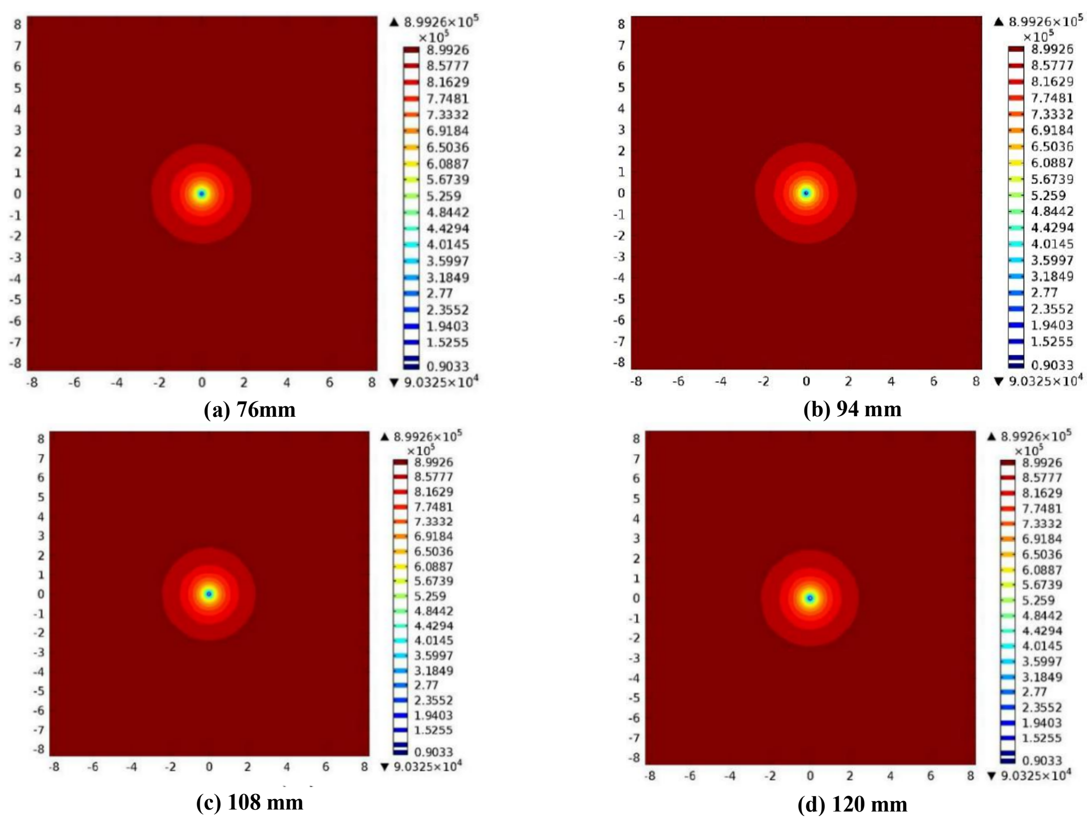

Figure13. Cloud map of gas pressure distribution under different borehole diameter conditions

To quantify the influence of borehole diameter, gas pressure profiles were extracted along a 15-m radial line extending from the borehole center. As shown in Figure 14, the pressure curves for boreholes with diameters of 76 mm, 94 mm, 108 mm, and 120 mm virtually coincide. This result demonstrates that gas pressure exhibits low sensitivity to changes in borehole diameter.

Consequently, within the diameter range studied (76 mm-120 mm), increasing the borehole diameter only induces a marginal alteration in the gas pressure field and does not materially improve gas drainage performance.

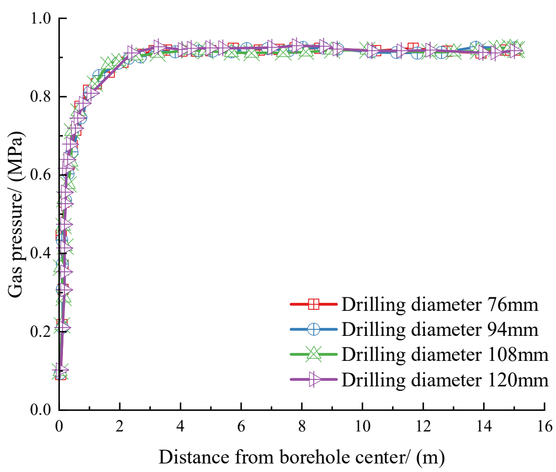

Figure14. Distribution of gas pressure around the borehole for different borehole diameters

4.2.3. Optimization of Cross-Measure Borehole Drainage Negative Pressure

Figure 15 presents the gas pressure distribution cloud map under different drainage negative pressure conditions. As observed in the figure, the variation in gas pressure distribution within the drainage area with respect to negative pressure is minimal-this indicates that drainage negative pressure has a weak influence on the overall gas pressure distribution.

This result suggests that, within the simulated negative pressure range (-10 kPa to -40 kPa), increasing the drainage negative pressure does not significantly improve gas drainage efficiency. Further analysis reveals that within a certain scope, significant variations in gas pressure are primarily driven by factors such as coal seam permeability and borehole layout, rather than by simply increasing the negative pressure. Therefore, when optimizing drainage system design, it is crucial to consider the synergistic effect between negative pressure regulation and the physical properties of the coal seam to achieve more efficient gas drainage.

Although the simulated negative pressure range (-10 kPa to -40 kPa) is lower than the on-site application range (-60 kPa to -90 kPa), on-site monitoring data from the 8235longwall face (2023) show that increasing the vacuum pressure from -40 kPa to -80 kPa results in an additional gas pressure drop of less than 5%. This confirms that gas drainage remains insensitive to negative pressure when the pressure exceeds -40 kPa.

To investigate the variation of gas pressure around the borehole under different drainage negative pressure conditions, this study took the borehole center as the origin and calculated/analyzed the gas pressure distribution within a 15-m extension along the radial positive direction.

As shown in Figure 16, the gas pressure distribution curves under different drainage negative pressure conditions are nearly identical. This result suggests that changes in drainage negative pressure have a minimal impact on gas pressure distribution. Specifically, within the simulated negative pressure range (-10 kPa to -40 kPa), a moderate increase in drainage negative pressure does not significantly alter the spatial distribution of gas pressure, nor does it induce substantial reductions in gas pressure.

4.3. Implications and Limitations

From a mechanistic perspective, the optimal 3-5 m depth layer in the floor strata coincides with the dilatant fracture zone, where permeability increases by more than 100-fold. Compared with roof high-level boreholes, the proposed cross-measure borehole layout reduces drilling footage by approximately 30%.

Economic analysis shows that this layout decreases the total borehole length by 18%, resulting in a cost saving of approximately USD 12,000 per 100 meters of longwall face. These parameters are valid for floor thicknesses of 12-30 m and coal seam permeabilities of 10^{-17}-10^{-16} m^2, covering 85% of the working panels at Qidong Coal Mine.

Limitations of this study primarily include the use of a 2-D geometric model and the assumption of linear-elastic coal behavior; future 3-D elastoplastic models will further refine these research results.

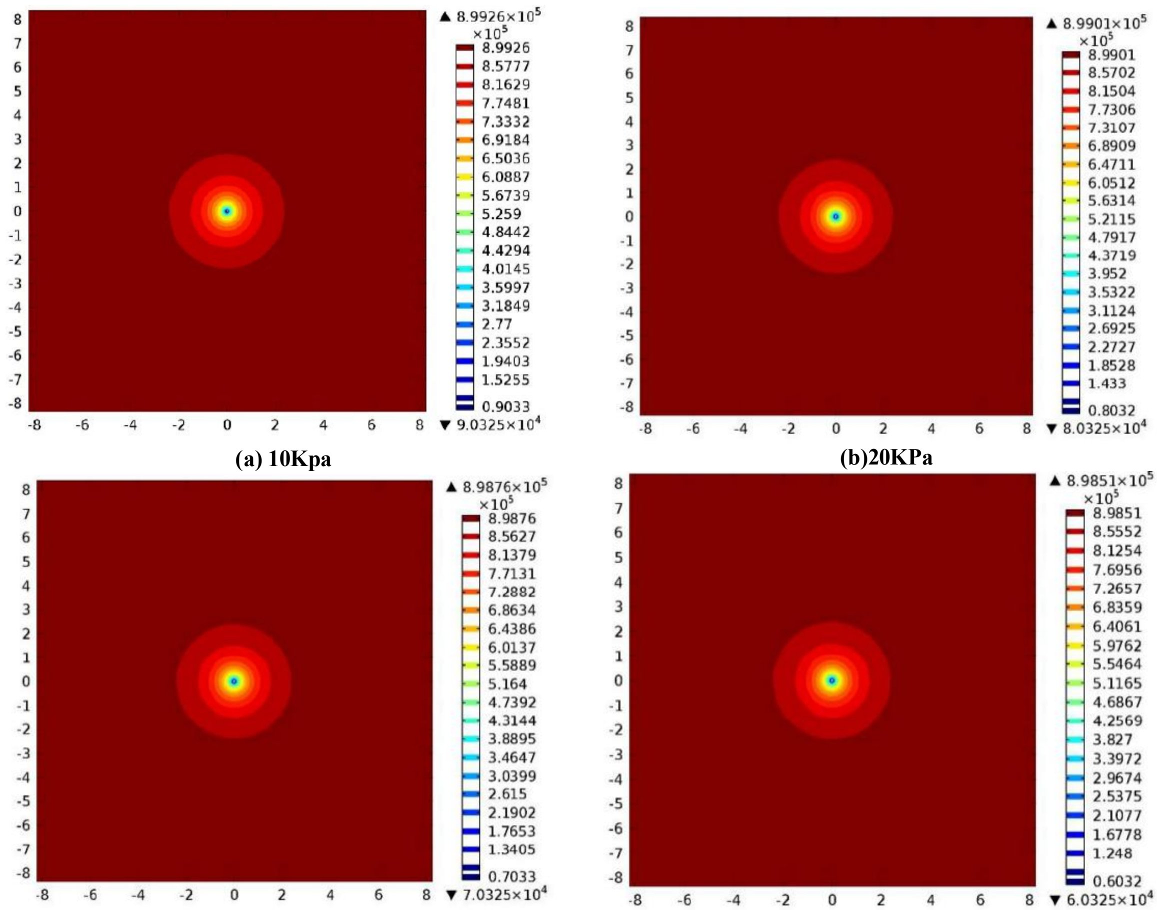

(a) 10Kpa **(b)20KPa**

(c) 30Kpa **(d)40KPa**

Figure15. Cloud diagram of gas pressure distribution under different drainage negative pressure conditions

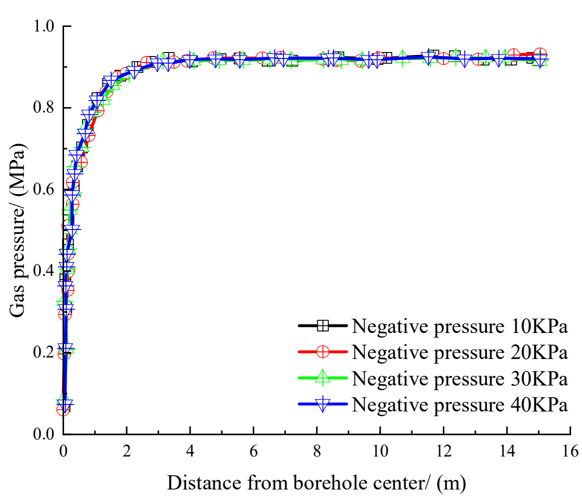

Figure16. Gas pressure distribution around the borehole under different negative drainage pressures

5. Conclusions

(1) In this study, numerical simulation and parameter optimization of directional boreholes were conducted for the 8237 and 8235 longwall faces using COMSOL Multiphysics (a multi-field coupling software). The results indicate the following: for the longwall face length, no fewer than four directional borehole sites should be established, with an interval of approximately 200 m between sites. Each site should be equipped with no fewer than five boreholes, resulting in a total of no fewer than 20 boreholes. Recommended borehole parameters are a diameter of Φ120 mm, a length of 550-650 m, and a spacing of 12-16 m. The drilling horizon should be 3-5 m above the roof of Coal Seam 9. Borehole azimuths should be 135°-145° for the opening section and approximately 100° for the final section. By coupling stress-permeability evolution, this study demonstrates that mining-induced fractures increase local permeability by two orders of magnitude. This, in turn, expands the effective drainage radius by approximately 35%, thereby establishing a quantitative link between fracture density and gas migration capacity.

(2) Following numerical simulation and optimization of floor cross-measure boreholes for the 8235longwall face, the recommended borehole spacing is 20-25 m. Specific layout requirements are

as follows: along No. 3 Gas Drainage Lane on the eastern flank, a fan-shaped array of at least six cross-measure boreholes should be installed every 25 m. The boreholes should be oriented perpendicular to the airway direction, with their inclination angles determined based on the final borehole spacing (25 m). Simulation results show that gas pressure is relatively insensitive to changes in borehole diameter and drainage negative pressure; moderate increases in these parameters do not significantly reduce gas pressure. Notably, the recommended optimal borehole spacing (20-25 m) corresponds to half the wavelength of the mining-induced fracture zone (approximately 40 m, verified by on-site micro-seismic data). This spacing ensures overlapping of drainage halos while minimizing redundant drilling work.

References

[1]. Raza, M. A., Karim, A., Aman, M. M., Al-Khasawneh, M. A., & Faheem, M. (2025). Global progress towards the Coal: Tracking coal reserves, coal prices, electricity from coal, carbon emissions and coal phase-out. *Gondwana Research, 139,* 43-72.

[2]. Chen, X., Li, L., Wang, L., & Qi, L. (2019). The current situation and prevention and control countermeasures for typical dynamic disasters in kilometer-deep mines in China. *Safety science, 115,* 229-236.

[3]. Wu, Y., Xiao, X., & Song, Z. (2017). Competitiveness analysis of coal industry in China: A diamond model study. *Resources Policy, 52,* 39-53.

[4]. Dzhioeva, A. K., & Brigida, V. S. (2020). Spatial non-linearity of methane release dynamics in underground boreholes for sustainable mining. *Записки Горного института, 245,* 522-530.

[5]. Tian, S., Wang, Y., Ma, T., Mao, J., & Ma, L. (2024). Analysis of the causes and safety countermeasures of coal mine accidents: A case study of coal mine accidents in China from 2018 to 2022. *Process Safety and Environmental Protection, 187,* 864-875.

[6]. Yuxin, W., Gui, F., Qian, L., Jingru, W., Yali, W., Meng, H., ... & Xuecai, X. (2024). Accident case-driven study on the causal modeling and prevention strategies of coal-mine gas-explosion accidents: A systematic analysis of coal-mine accidents in China. *Resources Policy, 88,* 104425.

[7]. Braga, L. T. P., & Kudasik, M. (2019). Permeability measurements of raw and briquette coal of various porosities at different temperatures. *Materials Research Express, 6*(10), 105609.

[8]. Li, H., Wang, W., Liu, Y., Ma, J., & Gao, H. (2020). An integrated drilling, protection and sealing technology for improving the gas drainage effect in soft coal seams. *Energy Reports, 6,* 2030-2043.

[9]. Yan, X., Ariaratnam, S. T., Dong, S., & Zeng, C. (2018). Horizontal directional drilling: State-of-the-art review of theory and applications. *Tunnelling and Underground Space Technology, 72,* 162-173.

[10]. Niu, X., Pang, D., Liu, H., Zhang, Y., Cheng, G., Cao, J., & Zhao, Y. (2023). Gas extraction mechanism and effect of ultra-high-pressure hydraulic slotting technology: A case study in Renlou coal mine. *Natural Resources Research, 32*(1), 321-339.

[11]. Zhai, C., Li, M., Sun, C., Zhang, J., Yang, W., & Li, Q. (2012). Guiding-controlling technology of coal seam hydraulic fracturing fractures extension. *International Journal of Mining Science and Technology, 22*(6), 831-836.

[12]. Hosseini, A., Najafi, M., & Hossein Morshedy, A. (2024). A 3D numerical model for improving methane drainage efficiency in underground coal mines using the cross-measure borehole method. *International Journal of Energy Research, 2024*(1), 6921566.

[13]. Hosseini, A., Najafi, M., & Morshedy, A. (2022). Determination of suitable distance between methane drainage stations in Tabas mechanized coal mine (Iran) based on theoretical calculations and field investigation. *Journal of Mining Institute, 258,* 1050-1060.

[14]. Hosseini, A., & Najafi, M. (2021). Determination of methane desorption zone for the design of a drainage borehole pattern (case study: E4 panel of the tabas mechanized coal mine, Iran). *Rudarsko-geološko-naftni zbornik, 36(1),* 61-75.

[15]. Hosseini, A., Najafi, M., & Morshedy, A. H. (2022). The effect of technical parameters of cross-measure boreholes methane drainage method on the amount of exhaust gas (Case study: Tabas Parvadeh coal mine No. 1). *Journal of Analytical and Numerical Methods in Mining Engineering*, *12*(30), 79-89.

[16]. Hosseini, A., Najafi, M., & Hossein Morshedy, A. (2025). Hybrid ANN-GWO Algorithm for Improving Methane Drainage Efficiency in Cross-Measure Borehole in Underground Coal Mines. *International Journal of Energy Research, 2025*(1), 1326901.

[17]. Bagherzadeh, A., Najafi, M., Marji, M. F., & Noroozi, M. (2022). A proper borehole pattern design for coal seam methane drainage in Tabas coal mine using Comsol Multiphysics. *Journal of Sustainable Mining, 21.*

[18]. Qin, M. (2017). Study on the treatment of upper corner gas based on the roof-drilling holes. In *Innovation and Application of Engineering Technology* (pp. 109-114). CRC Press.

[19]. Yeo, M., Macgregor, A. J., Pinkstone, H., & Piccolo, B. (2015, April). Offshore deepwater managed pressure drilling and riser gas handling equipment design. In *SPE/IADC Managed Pressure Drilling and Underbalanced Operations Conference and Exhibition* (pp. SPE-173819). SPE.

[20]. Zhang, J., Ruan, G., Bai, Y., & Ning, T. (2022). Mathematical Model and Numerical Simulation Study of the Mining Area with Multiple Air Leakage Paths. *Mathematics, 10*(14), 2484.

[21]. Ruda, T., & Farrar, J. (2005). Environmental drilling for soil sampling, rock coring, borehole logging, and monitoring well installation. In *Practical handbook of*

environmental site characterization and ground-water monitoring (pp. 307-354). CRC Press.

[22]. Majeed, G. A. M. (2020). *Directional Drilling Optimization with Mud Motor and Rotary Steerable System* (Doctoral dissertation, Politecnico di Torino).

[23]. Wood, D. A. (2015). Drilling and borehole techniques relevant to natural gas exploration and development: a collection of published research (2009-2015). *Journal of Natural Gas Science and Engineering, 26,* 396-408.

[24]. Yan, Z., Wang, Y., Fan, J., Huang, Y., & He, Y. (2021). Study on key parameters of directional long borehole layout in high-gas working face. *Shock and Vibration, 2021*(1), 5579967.

[25]. Chen, Y., Zhou, L., Peng, Y., & Ren, X. (2023). Numerical study on the effectiveness of a directional well with multiple hydraulic slots for enhanced gas recovery in deep coal seams. *Geomechanics and Geophysics for Geo-Energy and Geo-Resources, 9*(1), 138.

[26]. Li, Z., Xie, R., Wu, Y., & Yuan, J. (2022). Progress and prospects of CNOOC's oil and gas well drilling and completion technologies. *Natural Gas Industry B, 9*(2), 209-217.

[27]. Liu, J., Wu, Z., Lu, P., Liu, Z., & Su, M. (2023). Study on the effective extraction radius of directional long boreholes and analysis of the influence mechanism. *ACS Omega, 8*(2), 2344-2356.

[28]. Li, Y. (2018). Upper corner gas control based on high level directional long borehole. *Coal science and technology,* (1).

[29]. Chao, X. U., Fei, L. I. U., & Jun, F. A. N. G. (2017). Effect analysis of gas drainage with high level directional long drilling. *Coal Engineering, 49*(6), 78-81.

[30]. Jamalan, S., Sereshki, F., Ataei, M., & Najafi, M. (2022). Numerical modeling of coal gas drainage in a three-dimensional framework. *Arabian Journal of Geosciences, 15*(9), 826.

[31]. Tanguturi, K., & Balusu, R. (2015). Fundamental understanding of goaf gas displacement in longwall goaf. *Journal of mining and environment, 6*(2), 191-203.

[32]. Hosseini, M., Madani, H., & Shahriar, K. (2022). CFD-based modeling of sarin gas dispersion in a subway station-A hypothetical scenario. *Journal of Mining and Environment, 13*(1), 235-251.

[33]. Li, C., Li, C., Nie, B., Han, Q., & Cao, J. (2024). Effect of anchor shear deformation on the propagation rules of excitation stress waves. *Scientific Reports, 14*(1), 29995.

[34]. Wang, X., Zhang, Y., Zhang, Q., Wei, Y., Liu, W., & Jiang, T. (2022). Space-time evolution characteristics of deformation and failure of surrounding rock in deep soft rock roadway. *Sustainability, 14*(19), 12587.

[35]. Zhang, J., Dong, Y., Chen, Y., Jiang, Y., Sun, H., Fan, Y., & Wang, C. (2018). Comparative Analysis of Roadway Reinforcement Effects Based on Fluid-Solid Coupling in the Fractured Zone of Water-Rich Fault. *Advances in Civil Engineering, 2018*(1), 6238910.

[36]. Guanghong, W. A. N. G. (2019). Application test on pre-drainage strip gas in coal roadway based on floor directional long borehole technology. *China Energy and Environmental Protection*, *41*(5), 1-4.

[37]. Wang, F., Ren, T., Tu, S., Hungerford, F., & Aziz, N. (2012). Implementation of underground longhole directional drilling technology for greenhouse gas mitigation in Chinese coal mines. *International Journal of Greenhouse Gas Control, 11,* 290-303.

[38]. Evanoski-Cole, A. R., Gebhart, K. A., Sive, B. C., Zhou, Y., Capps, S. L., Day, D. E., ... & Collett Jr, J. L. (2017). Composition and sources of winter haze in the Bakken oil and gas extraction region. *Atmospheric Environment, 156,* 77-87.

[39]. Field, R. A., Soltis, J., & Murphy, S. (2014). Air quality concerns of unconventional oil and natural gas production. *Environ-mental Science: Processes & Impacts, 16*(5)*,* 954-969.

[40]. Liu, J., Wang, Z., Wang, Q., Zou, S., & Yang, X. (2024). Study on the application of comprehensive gas control technology for Source-Separated Three-Dimensional gas extraction in large mining faces. *ACS omega*, *9*(30), 32777-32788.

[41]. Robertson, E. P., & Christiansen, R. L. (2008). A permeability model for coal and other fractured, sorptive-elastic media. *Spe Journal*, *13*(03), 314-324.

[42]. Pan, Z., & Connell, L. D. (2011). Modelling of anisotropic coal swelling and its impact on permeability behaviour for primary and enhanced coalbed methane recovery. *International Journal of Coal Geology*, *85*(3-4), 257-267.

[43]. Chen, L., Ma, M., Wang, H., Liu, X., Wu, M., & Hirota, K. (2025). Lithology identification of coal-bearing strata based on data-driven dual-channel relevance networks in coal mine roadway drilling process. *Information Sciences*, *690*, 121339.

[44]. Cui, P. F., Shang, D. L., Chu, P., Li, J., Sun, D. L., Wang, T. Y., ... & Xie, H. P. (2024). Optimal depth of in-situ pressure-preserved coring in coal seams considering roadway excavation and drilling disturbance. *Petroleum Science*, *21*(5), 3517-3534.

انجمن مهندسی معدن ایران
نشریه مهندسی معدن و محیط زیست
نشانی نشریه: www.jme.shahroodut.ac.ir
دانشگاه صنعتی شاهرود

بهینه‌سازی پارامتری زهکشی متان از طریق گمانه‌های اندازه‌گیری متقاطع در لایه‌های کف یک معدن زغال سنگ: یک مطالعه شبیه‌سازی چندفیزیکی

تینگزه لی[1]، یو وانگ[2]، و جنیوان تان[3]*

۱ .دانشکده علوم زمین و مهندسی، دانشگاه جنوب غربی جیائوتونگ، چنگدو، سیچوان، چین

۲ .دانشکده منابع و علوم زمین، دانشگاه معدن و فناوری چین، شوژو، جیانگ سو، چین

۳. کالج مهندسی ایمنی، دانشگاه معدن و فناوری چین، شوژو، جیانگ سو، چین

اطلاعات مقاله

تاریخ ارسال: ۲۰۲۵/۰۸/۱۹

تاریخ داوری: ۲۰۲۵/۱۰/۱۰

تاریخ پذیرش: ۲۰۲۶/۰۱/۰۴

DOI: 10.22044/jme.2026.16664.3273

کلمات کلیدی

کنترل گاز معدن زغال سنگ

لایه‌های کف

اندازه‌گیری متقاطع گمانه‌ها

بهینه‌سازی پارامتر گمانه

جفت شدن تنش-نفوذپذیری

چکیده

تخلیه مؤثر گاز در معادن زغال سنگ، بهینه‌سازی دقیق پارامترهای گمانه را برای کاهش فشار گاز و جلوگیری از فوران گاز ضروری می‌سازد. با این حال، طرح‌های حفاری فعلی عمدتاً به جای تجزیه و تحلیل کمی شرایط زمین‌شناسی خاص محل، به تجربه میدانی متکی هستند که منجر به محدودیت‌هایی در سازگاری می‌شود. این مطالعه یک مدل کوپلینگ چندفیزیکی مبتنی بر COMSOL ایجاد می‌کند که برهمکنش‌های تنش-نفوذپذیری، سینتیک جذب-واجذب گاز و تکامل نفوذپذیری ناشی از شکستگی را برای ارزیابی عملکرد تخلیه گاز گمانه‌های اندازه‌گیری متقاطع در لایه‌های کف ادغام می‌کند. نتایج شبیه‌سازی نشان می‌دهد که فاصله گمانه‌های جهت‌دار تأثیرگذارترین عامل است: کاهش فاصله از ۲۵ متر به ۲۰ متر، راندمان تخلیه گاز را به طور قابل توجهی ۳۱.۴٪ افزایش می‌دهد، در حالی که افزایش مدت زمان تخلیه از ۹۰ روز به ۲۷۰ روز، شعاع نفوذ را بیش از ۳۵٪ افزایش می‌دهد. در مقابل، تغییرات در قطر گمانه (۷۵-۱۱۵ میلی‌متر) و فشار منفی (۱۰-۹۰ کیلوپاسکال) تأثیر ناچیزی بر فشار گاز (با تغییر کمتر از ۵٪) دارند که نشان‌دهنده حساسیت محدود است. محل بهینه گمانه در مرز پایینی ناحیه شکستگی ناشی از معدنکاری تعیین شده است. تجزیه و تحلیل لایه گرادیان همچنین تأیید می‌کند که عمق سوراخکاری باید با محدوده ناحیه تغییر شکل پلاستیک (۱۵-۲۵ متر) مطابقت داشته باشد. استراتژی بهینه‌سازی پارامتری پیشنهادی، یک چارچوب کمی برای طراحی حفاری جهت‌دار ارائه می‌دهد و امکان تطبیق طرح گمانه با مقیاس توسعه شکستگی را فراهم می‌کند. این یافته‌ها به افزایش دقت کنترل گاز و سازگاری مهندسی سیستم‌های زهکشی گاز در شرایط پیچیده زمین‌شناسی کمک می‌کند.

نویسنده مسئول مکاتبات: *18955462692@163.com* (ج. تان)